RSC Advances

This article can be cited before page numbers have been issued, to do this please use: S. Wang, Z. Huo, K. Liu, N. Yu, Y. Ma, Y. Qin, X. Li and Z. Wang, *RSC Adv.*, 2015, DOI: 10.1039/C5RA09931E.

ROYAL SOCIETY OF CHEMISTRY

www.rsc.org/advances

View Article Online
DOI: 10.1039/C5RA09931E

A Ligand-conjugated pH-sensitive Polymeric Micelles for the Targeted Delivery of Gefitinib in Lung cancers

Shi-Jiang Wang [1], Zhi-Jun Huo[2], Kai Liu[3], Ning Yu[4], Yan Ma[1], Yue-Hong Qin[5], Xiao-Chen Li[6], Zhi-Qi Wang[7]*

[1]Department of Radiation Oncology, Shandong Cancer Hospital and Institute, Ji'nan, Shandong, 250117, China
[2]Department of Breast Disease Center, Shandong Cancer Hospital and Institute, Ji'nan, Shandong, 250117, China
[3]Department of Gastrointestinal Surgery, Shandong Cancer Hospital and Institute, Ji'nan, Shandong, 250117, China
[4]Department of pathology, Affiliated hospital of Binzhou medical college, Binzhou, Shandong, 256603, China
[5]Department of Neurosurgery, Shandong Provincial Hospital, Ji'nan, Shandong, 250021, China
[6]Department of Internal Medicine, Affiliated Hospital of Shandong Academy of Medical Sciences, Ji'nan, Shandong, 250021, China
[7]Department of Head and Neck Surgery, Shandong Cancer Hospital and Institute, Ji'nan, Shandong, 250117, China

Corresponding author:
Zhi-Qi Wang,
Department of Head and Neck Surgery,
Shandong Cancer Hospital and Institute,
No.440, Ji Yan Road, Jinan, 300162, Shandong, P.R.China
Tel & Fax: 0086-0531-67626141
Email:wzqbansg@hotmail.com

View Article Online
DOI: 10.1039/C5RA09931E

Abstract

The aim of present study was to investigate the tumor targeting potential of mannose-conjugated pH-sensitive nanosystem for the effective delivery of Gefitinib (Gnb) to lung cancers. We have successfully demonstrated the prospective of mannose-tagged nanomicelles as an efficient vector to ferry anticancer drug. The micelles exhibited a nanosized particle with excellent dispersity index. The nanomicelles exhibited a pH-responsive nature with enhanced drug release in the acidic pH conditions. The fluorescence and flow cytometer analysis showed a superior cellular uptake for mannose-tagged nanomicelles. The CLSM study revealed a receptor-mediated cellular internalization process. The M-NP-Gnb showed a superior anticancer effect in A549 cancer cells and remarkably inhibited the cancer cell proliferation. Furthermore, M-NP-Gnb significantly increased the proportion of cells in the apoptosis and necrosis region. Importantly, half-life of Gnb encapsulated in nanomicelles increased by about 5-fold comparing to that of free Gnb. The augmented half-life clearly indicates the maximum residence time of drug in the systemic circulation. Consistently, M-NP-Gnb showed a 7-fold higher accumulation of drug in tumor tissues compared to that of free Gnb. Overall; PLGA/His-based nanomicelles could be a promising delivery system to increase the therapeutic efficiency of Gnb in lung cancers.

Keywords

Lung cancers, apoptosis, gefitinib, nanomicelles, pH-sensitive

View Article Online
DOI: 10.1039/C5RA09931E

Introduction

Lung cancer is one of the leading causes of cancer-related death worldwide. The death rate due to lung cancer far exceeds the death rate of prostate, colon, and breast cancers united.[1,2] The 5-year survival rate of lung cancer patients are below 15% despite the advancement in technological field. The lung cancers could be divided into non-small cell lung cancer (NSCLC) and small cell lung cancer (SCLC).[3] Non-small cell lung cancer (NSCLC) comprises approximately 75–80% of all respiratory lung cancers. The incidence and mortality of lung cancer are increasing every year in China. At present, surgery, radiotherapy and chemotherapy constitutes the main treatment mode for lung cancers.[4,5]

In this regard, tyrosine kinase inhibitors are shown to possess excellent antitumor activity against lung cancer cells. Gefitinib (Gnb), a tyrosine kinase inhibitor has high affinity towards epithelial growth factor receptor (EGFR) which is normally expressed in lung cancers.[6,7] Gnb can effectively kill lung cancer cells via promoting metastasis, angiogenesis, and apoptosis in tumor cells. The main mechanism behind the anticancer effect of Gnb is by blocking the signal transmission by competitive binding Mg-ATP situated on the catalytic domain of EGFR-TK.[8,9] This will inhibit the activation of mitogen activated protein kinase and induce the apoptosis of cancer cells. Despite its potential clinical application, Gnb is widely distributed in the body and results in severe drug-related toxicity. Moreover, limited presence of drug in the cancer cells further complicates the chemotherapy treatment.[10] Therefore, new strategies have to be developed to increase the chemotherapeutic efficacy of Gnb in lung cancers.

Nanotechnology has opened up new horizons in cancer drug delivery. Recent studies have highlighted the role of nanotechnology in cancer therapy.[11] Drug-loaded nanocarriers have been

View Article Online
DOI: 10.1039/C5RA09931E

shown to increase the blood circulation of the anticancer small molecules, sustained the drug release in the physiological conditions, and increased its accumulation in the tumor region.[12] When antitumor drugs are loaded in nanoparticles with the size of 20–200 nm, their biodistribution in heart and lung is largely decreased.[13] In this study therefore, a novel pH-sensitive delivery system has been designed that will increase the drug concentration in the cancer tissues while reducing its presence in the normal tissues. PLGA is one of the most common polymers used as carrier for drug delivery applications due to inherent biodegradability and low toxicity. Therefore, PLGA-PEG was selected in order to form a stable hydrophobic core and PEG forms the outer shell which protects the carrier from immediate systemic clearance. Poly-histidine was synthesized and utilized in micelle formation in order to bring the pH-responsiveness to the carrier system.[14,15] The so formed nanocarrier is able to extravasate solid tumors into the tumor tissues via enhanced permeability and retention effect (EPR). However, passive targeting of cancer cells is not found to be effective and warranted alternative therapeutic approach.[17,18] In this context, glycotargeting involves the interaction of lectin receptors to the carbohydrate ligands. It has been reported that mannose-cytostatics complexes exhibits selective uptake in cancer cells.[19] The preferential uptake was attributed to the receptor-mediated internalization by lectin receptors at the tumor surface. In the present study therefore, polysaccharide-mannose tagged PLGA-based nanocarrier system has been developed to target lung cancers.[20]

The main objective of present study was to explore the prospective of polysaccharide tagged pH-sensitive nanomicelles (PLGA/Histidine) for the selective delivery of gefitinib in lung cancers. In this study, we firstly developed PLGA/pHistidine-based nanomicelles which were then conjugated with mannose as a cancer targeting moiety. The pH-sensitive nature of nanocarrier

View Article Online
DOI: 10.1039/C5RA09931E

was asserted by means of particle size analysis and drug release kinetics study. In vitro cellular uptake of targeted and non-targeted NP was analyzed by fluorescence and flow cytometry (FACS) and observed by confocal laser scanning microscopy (CLSM). The methylthiazoltetrazolium (MTT) assay was employed to examine the in vitro cytotoxicity of the free drug as well as drug-loaded micelles. Annexin V/PI-based apoptosis analysis was performed in A549 lung cancer cells. Finally, systemic performance of free drug and drug-loaded micelles were performed in experimental rats.

Results and Discussion

Lung cancer is one of the leading causes of cancer-related death worldwide. In this regard, Gefitinib (Gnb), a tyrosine kinase inhibitor could effectively kill lung cancer cells via promoting metastasis, angiogenesis, and apoptosis in tumor cells. Therefore, in the present study, we have developed PLGA/pHistidine-based nanomicelles to target the Gnb to lung cancer cells (Figure 1).

Preparation of M-NP-Gnb nanomicelles

The pHIS-PEG was synthesized by ring opening polymerization process. The poly (L-histidine) was conjugated with PEG via an amide bond. In case of PLGA-PEG-NH2, PEG-diamine was reacted with the PLGA-NHS and resulting product was reacted with mannose. The mannosylation was performed by ring opening of mannose and subsequent reaction of its aldehyde group with free amine functional group of PLGA-PEG-NH2 of the nanoparticle surface. This leads to the formation of Schiff's base (-N-CH-). The main objective of present study was to explore the prospective of polysaccharide tagged pH-sensitive nanomicelles

View Article Online
DOI: 10.1039/C5RA09931E

(PLGA/Histidine) for the selective delivery of gefitinib in lung cancers. The PLGA-PEG and Histidine-PEG was synthesized in order to formulate mixed micelles wherein PLGA will form the inner hydrophobic core and PEG forms the outer shell. The mannose was conjugated to PLGA-PEG polymer block and present in the outer nanoparticle surface. The presence of mannose on the outer nanoparticle surface will increase the targeting and accumulating efficiency of chemotherapeutic drug.

Characterization of M-NP-Gnb

The particle size and zeta potential of all the nanoparticles were evaluated by dynamic light scattering method. The average particle size of NP-Gnb was about 120 nm and the particle size increased for the mannose conjugation (168 nm) (Figure 2a). The increase in the size of nanoparticles was due to the presence of mannose conjugation to the outer surface. Nevertheless, particle size of <200 nm would be much suitable for tumor targeting applications.[21] The micelles were negative charged with -18.5 mV. The negative surface charge of nanoparticles would increase the physiological stability in the blood circulation. During in vivo applications, negative surface charge would reduce the undesirable clearance by reticuloendothelial system (RES) which would increase its accumulation in the tumor tissues. The particle morphology was observed using TEM imaging. TEM showed clear spherical shaped particles for M-NP-Gnb which is uniformly dispersed in the carbon-coated copper grid (Figure 2b). The particle size observed form TEM imaging was consistent with the DLS particle size.

pH-sensitivity of M-NP-Gnb micelles

The pH-sensitive nature of M-NP-Gnb was investigated by means of size, size distribution, and zeta potential analysis. The histidine present in the micellar structure is mainly responsible for

View Article Online
DOI: 10.1039/C5RA09931E

the pH-responsiveness of the system. As shown in Table 1, zeta potential increased with the decrease in the pH of suspended medium indicating the effective protonation of the histidine residue. Especially, micelles were stable at pH 7.4, however when the pH decreased to 5.5, abundant protonation of histidine resulted in low zeta potential of -3 mV. Consistently, particle size of the micelles increased due to the disassembly and aggregation of the multiple polymers.

Drug loading and in vitro drug release study

Knowledge of drug entrapment efficiency is very important for drug delivery applications. The M-NP-Gnb exhibited a high entrapment efficiency of >95% with a high drug loading of ~24.7%. The pH-sensitive nature of NP-Gnb and M-NP-Gnb was evaluated from the release kinetics. It is expected that presence of Histidine in the mixed micelle would provide the pH-responsive nature to the nanocarrier system. The pH-responsiveness would increase the swelling and dissociation of micellar system resulting in the release of drug. It can be seen from Figure 3 that both NP-Gnb and M-NP-Gnb exhibited a typical pH-sensitive release pattern. Approximately, 60% of drug released in pH 5.5 conditions compared to 35% of drug released in pH 7.4 conditions. The release trend continued up to 48h where in almost 95% of drug released in acidic pH and 50% of drug released in pH 7.4 conditions. It should be noted that no initial burst release phenomenon was observed suggesting that all of drug were tightly packed in the hydrophobic core of micelles. Although the rate of drug release from NP-Gnb and M-NP-Gnb was almost similar, a slight decrease in the release rate from M-NP-Gnb was ascribed to the presence of the protective coat of mannose on the SLNs surface, which impedes the drug release.[22] Overall, enhanced release

View Article Online
DOI: 10.1039/C5RA09931E

rate at lower pH would be beneficial for anti-cancer application since tumor tissue is characterized by an acidic microenvironment

Cellular uptake efficiency

The cellular uptake efficiency as a function of targeting agent has been studied on CHO (control cells) and A549 lung cancer cells. For this purpose, rhodamine-b was loaded in the nanomicellar formulations to observe the fluorescence intensity or fluorescence measurement. The cellular uptake of targeted and non-targeted nanoparticles was studied in these two cell lines by means of flow cytometer (Figure 4a). In case of CHO cells (which don't express lectin receptors), cellular uptake of NP and M-NP-Gnb were not markedly different. In case of A-549 cells however, remarkable difference were observed between targeted and non-targeted nanoparticles. It could be clearly seen that M-NP-Gnb had significantly higher cellular uptake than NP after 2h of incubation. The mannose-tagged micelles could enter the cells more quickly than the non-targeted NP. Mannosylated NP's could not be taken up by CHO cells via receptor-mediated endocytosis because mannose receptors are not expressed on their membrane. Having shown the specificity of mannosylated NP towards lectin receptor expression cancer cells, we have carried all our experiments in A-549 cells.

The cellular uptake was further studied by fluorescence experiments. The cancer cells were exposed with NP-Gnb and M-NP-Gnb and incubated for different time period up to 4h (Figure 4a). The results clearly revealed a time-dependent cellular uptake. Importantly, mannose-tagged formulations showed a significant increment in the cellular uptake compared to that of non-targeted nanosystem. For example, at the end of 4h, M-NP showed ~70% fluorescent intensity compared to that of ~38% fluorescent intensity of non-targeted NP. The high fluorescent

View Article Online
DOI: 10.1039/C5RA09931E

fluorescence intensity associated with the M-NP system was mainly attributed to the lectin receptor-mediated internalization of nanomicelles. It could be noticed that non-targeted NP also showed some uptake which is possibly due to the endocytosis mediated non-specific internalization.[23] Such high uptake of mannose-targeted system could increase the intracellular concentration as well the cytotoxic effect of the anticancer cancer drugs.

Cellular internalization

The result from the cellular uptake analysis indicates the mannose-tagged nanomicelles could effectively internalize the cancer cells than the non-targeted nanomicelles. We further investigated the mechanism of cellular uptake in A549 cancer cells. CLSM was used to evaluate the cellular uptake. For this purpose, we have stained the lysosome with Lysotracker Green (green color) and nucleus was stained with DAPI (blue color). As mentioned above, nanomicelles were loaded with rhodamine-b to impart the fluorescence intensity. As seen (Figure 5), M-NP treated cells showed bright red fluorescence compared to that of NP treated cell group indicating the enhanced cellular internalization in case of ligand-tagged formulations. The M-NP was very well colocalized in the lysosomal region indicating a typical lectin receptor-mediated endocytosis uptake. In contrast, NP did not colocalize appreciably due to simple gradient-mediated uptake mechanism. It could expect that nanomicelles are triggered in the acidic endosomal/lysosomal compartments and leave endosomal/lysosomal compartments via simple diffusion to the nuclear region. Earlier, it has been reported that micellar formulations were internalized by caveolae-dependent manner wherein nanoparticles rapidly colocalize in the acidic compartments and the released drug will be travelling to the nuclear region.

View Article Online
DOI: 10.1039/C5RA09931E

Cytotoxicity assay

The cytotoxic potential of free Gnb and Gnb-loaded nanomicelles were evaluated by means of MTT assay. The results clearly showed a time-dependent and concentration-dependent cytotoxic action of Gnb (free and encapsulated form) in A549 lung cancer cells. The cytotoxic potential of different formulations was consistent with the cell uptake assays (Figure 6a,b). The IC50 value was calculated to quantitate the cytotoxic action of individual formulations. The IC50 value (the concentration that inhibited cell growth by 50%) of M-NP-Gnb was 0.85 µg/ml comparing to 2.35 µg/ml for NP-Gnb and 4.12 µg/ml for free Gnb after 24h incubation. The superior cytotoxic action of M-NP-Gnb was mainly attributed to the ligand-receptor interactions. The enhanced internalization, high accumulation of nanomicelles due to lectin-mannose interaction, sustained release characteristics of formulations within the cells could be responsible for the augmented cytotoxic effect.[24]

The Hoechst staining was carried out to observe the cellular morphology. As seen, control cells were intact with clear morphology (Figure 6c). The drug treatment however induced remarkable changes in cell morphology. Especially, M-NP-Gnb showed marked changes in cellular and nuclear morphology, including chromatin condensation, membrane blebbing, nuclear breakdown, and the appearance of membrane-associated apoptotic bodies.

Apoptosis assay

The apoptosis effect of individual formulations was studied by FACS analysis using Annexin V/PI staining (Figure 7). The results clearly showed that number of apoptotic and necrotic cells increased upon treatment with the formulation. The free Gnb slightly induced cell apoptosis with marginal amount of cells in the necrotic. The NP-Gnb however showed higher percentage of

View Article Online
DOI: 10.1039/C5RA09931E

cells in the apoptosis and necrotic region. Notably, M-NP-Gnb showed significantly higher proportions of cells in the apoptosis and necrotic stage indicating the superior anticancer effect of mannose-tagged formulations. The enhanced apoptosis of cancer cells were consistent with the higher cellular internalization and higher cell killing effect.

Pharmacokinetic and Biodistribution analysis

The pharmacokinetic study has been performed to investigate the systemic performance of free drug as well the drug-loaded nanomicelles. The in vivo study clearly revealed that pharmacokinetics of free drug significantly altered after encapsulation in the nanomicelles. As seen (Figure 8a), free Gnb was immediately cleared from the systemic circulation within 4-6h. The NP-Gnb and M-NP-Gnb significantly prolonged the residence time of Gnb up to 24h. The half-life of Gnb encapsulated in nanomicelles increased by about 5-fold comparing to that of free Gnb. The augmented half-life clearly indicates the maximum residence time of drug in the systemic circulation. The AUC_{0-24} and $AUC_{0-\infty}$ values of free DOX (18.45µg h/mL), NP-Gnb (65.92µg h/mL) and M-NP-Gnb (68.12µg h/mL) further demonstrated the long circulation property of nanomicelles. The long circulation property of NP-Gnb and M-NP-Gnb was attributed to the presence of PEG on the outer surface of nanocarrier. The PEG will effectively evade the macrophage uptake and augment the half-life of drug in the nanocarrier system. The prolonged blood circulation profile of mannose-conjugated nanomicelles would be crucial for tumor targeting. The M-NP-Gnb would be preferentially accumulated in tumor tissues via receptor-mediated endocytosis in mannose receptor overexpressed A549 tumor tissues.

The biodistribution study was conducted to further investigate the targeting ability of mannose-targeted nanosystem. As shown in Figure 8b, significantly higher concentration of Gnb was

View Article Online
DOI: 10.1039/C5RA09931E

accumulated in tumor tissues from M-NP-Gnb therapeutic system across all the time points. Approximately, 7-fold higher accumulation of drug was observed in tumor tissues than comparing to free drug. At the end of 24h, ~10 ng/gm of tissue was observed in M-NP-Gnb treated mice group whereas none was observed for free drug treated group. The ability of M-NP-Gnb to localize preferentially in the tumor tissue indicates its reduced entry on other vital organs. Moreover, it should be noted that drug level in M-NP-Gnb treated group kept increasing until 4h. This may be explained on the basis of the presence of lectin receptors on tumor tissues that favored selective entry of M-NP-Gnb in tumors. The presence of lectin receptors on the tumor surface presents an interesting platform and facilitates targeting. This strategy will help to augment the therapeutic effectiveness by lowering the dose of therapeutic moiety.

Materials and Methods

Materials

PLGA ([η] = 0.32–0.44 dL/g; 50:50) and d-mannose was purchased from Sigma-Aldrich (China). PEG-diamine was purchased from Laysan Bio Inc (Arab, AL). 1-ethyl-3 (3-dimethylaminopropyl) carbodimide (EDC) was purchased from Sigma Aldrich, China. N-(t-butyloxycarboryl)-1-(2,4-dinitrophenyl)-L-Histidine [Boc-His(DNP)-OH] was purchased from Sigma Aldrich (St, Louis, USA). All other chemicals were of reagent grade and used as such without further modification.

Preparation of Gefitinib-loaded nanomicelles

View Article Online
DOI: 10.1039/C5RA09931E

The PLGA-PEG polymer block was fabricated using carbodiimide chemistry. In brief, PLGA (10 g) was dissolved in DMSO and to this solution, EDC/NHS was added and the reaction was allowed to continue for 24h. The so-formed PLGA-NHS was collected by the addition of cold ether and filtered. The PLGA-NHS was reacted with PEG diamine at a ratio of 6:1 in DMSO and further stirred for 20h at room temperature. The final product PLGA-PEG-NH2 was precipitated by excessive acetonitrile and washed with diethyl ether. The unreacted PEG-diamine was separated by dialysis method. The final product Folate–PEG–PLA was obtained by freeze-drying and stored in refrigerator (4°C).[26]

mPEG-PolyHistidine was synthesized from the precursor Boc-His(DNP)-OH. In brief, 10 g of Boc-His(DNP)-OH was dissolved in dioxane and dichloro sulfoxide was added and stirred for 1h. The so-formed DNP-NCA-HCl was obtained after washed being by dioxane and dried in vacuum. Now, specific amount of DNP.NCA.HCl was reacted with sodium carbonate in DMF solution for 1h. The mPEG-NH2 (in DMF) was then added drop-wise to the above mixture and stirred for 48h at room temperature. The so-formed mPEG-Poly(Nim-DNP-histidine) was obtained after filtrated and dried in vacuum. Then, mPEG-Poly(Nim-DNP-histidine) (0.5g) was dissolved in 8 ml of DMSO and reacted with 2–mercaptoethanol and reacted for 12h at room temperature. The final product mPEG-PolyHistidine was obtained after filtrated and washed with ethanol and ether. The isolated product was dialyzed against distilled water (molecular weight cut-off (MWCO) = 3500 Da), and then freeze-dried to give the final product. [27]

The precipitate was redissolved in DMF The drug-loaded nanomicelles were prepared by dialysis method. Briefly, Gnb (5 mg), PLGA-PEG-NH2 (20 mg), pHIS–PEG (10 mg) was dissolved in 4 ml of DMSO and stirred for 20h.The solution was then dialyzed in a large quantity of water (dialysis membrane Mw~3500) for 48h. The drug-loaded nanomicelles was collected and

View Article Online
DOI: 10.1039/C5RA09931E

subsequently conjugated with d-mannose. D-mannose (10 μM) was dissolved in sodium acetate buffer (pH 4.0) and stirred for 24h. The mannosylated nanomicelles were further dialyzed for 48h to remove the unconjugated mannose. The final product was collected and purified as mentioned above and stored at cold temperatures.

Particle size and zeta potential analysis

The particle size, size distribution, and zeta potential surface charge of nanomicelles were evaluated by photon correlation spectroscopy (PCS) method. Zetasizer (Malvern Instruments, England) was used to measure the particle size and zeta potential. Samples were suitably diluted and analyzed at a fixed angle of 90°. For zeta potential measurement, the samples were diluted with phosphate buffered saline (pH 7.4).

In vitro release study

The drug release profile of Gnb from M-NP-Gnb and NP-Gnb was evaluated by means of dialysis method. For this purpose, 1 mg equivalent of Gnb in formulations were loaded in a dialysis tube (MW~3500 Da), sealed at both the end and suspended in a Falcon tube containing 20 ml of release media containing 1% Tween 80 to increase the solubility of drug in the medium. The medium was continuously stirred at 100 rpm and the whole assembly was placed at 37°C. At specific time point, samples were withdrawn from the medium and replaced with equal amount of fresh release medium. The samples were analyzed using HPLC method. Shimadzu HPLC system consisting of C-18 column was used. 0.02M dipottasium hydrogen ortho phosphate and methanol at a fixed ratio of 10:90 was used as a mobile phase. The mobile phase was run at 1 ml/min and quantified at 246 nm.

View Article Online
DOI: 10.1039/C5RA09931E

Cell viability assay

A549 lung epithelial cancer cell line was cultured in DMEM medium supplemented with 10% heat-inactivated fetal bovine serum (FBS), 1% streptomycin, 3 mM glutamine in a 37°C humidified incubator and 5% CO2 atmosphere. The cell viability of A549 cancer cell was investigated using 3-(4,5-dimethylthiazol-2-yl)-2,5- diphenyltetrazolium bromide (MTT) assay. The cells were seeded into 96-well plate at a density of 5×10^4 cells per well and allowed to attach for 24h at 37°C. The cells were then treated with free Gnb, NP-Gnb and M-NP-Gnb and incubated for 24h and 48h, respectively. The media was removed and washed twice with PBS buffer. Cells were treated with MTT solution (10 mg/mL) and incubated for 4 h at 37 °C, facilitating MTT to be reduced by viable cells with the formation of purple formazan crystals. DMSO was added to each well to dissolve the formazan crystals and the absorbance of individual wells was noted at 570 nm using an ELISA plate reader.

Cellular uptake analysis

The cellular uptake of targeted and non-targeted nanomicelles was determined by fluorescence microscopy. Briefly, cells were seeded in 96-well plate, allowed to attach, and exposed with rhodamine-b loaded NP and M-NP. The formulations were incubated in a time-dependent manner. The cells were washed twice with PBS to remove the nanocarriers adhering on the cell surface. The uptake was calculated from the absorbance of individual wells which was noted at 570 nm via an ELISA plate reader.

The cellular uptake was further confirmed by fluorescence activated cell sorters (FACS) instrument (BD Biosciences FACS Aria, Germany). Briefly, cells were seeded in 96-well plate, allowed to attach, and exposed with rhodamine-b loaded NP and M-NP. The formulations were

View Article Online
DOI: 10.1039/C5RA09931E

incubated in a time-dependent manner. The cells were washed and trypsinized (0.1% w/v). The cells were pelleted by centrifuging at 1200 rpm/5 min. The pellets were again re-dispersed in PBS buffer and cell-associated fluorescence was measured by fluorescence activated cell sorters (FACS) instrument.

Cell apoptosis analysis

The apoptosis effect of individual formulation was evaluated by Annexin-V/PI double staining assay using flow cytometer. The A549 cells were seeded in a 12-well plate and incubated overnight. Following day, cells were exposed with free Gnb, NP-Gnb and M-NP-Gnb formulations and incubated for 18h. Untreated cells were considered as a control. Next day, cells were washed with PBS twice, extracted, and re-suspended with binding buffer. Cells were then treated with 5 μL of Annexin V-FITC and 5 μL of propidium iodide for 5 minutes in the dark at room temperature, and apoptosis was then detected by flow cytometry (BD Biosciences FACS Aria, Germany).

Qualitative apoptosis analysis

The A549 cells were seeded in a 12-well plate (2×10^5 cells/well) and treated with free Gnb, NP-Gnb and M-NP-Gnb formulations and incubated for 24h. The cells were fixed and exposed with Hoechst 33382 nuclear staining dye. The cellular and nuclear morphology was observed using a fluorescence inversion microscope.

Cellular internalization

The cellular internalization of targeted and non-targeted nanomicelles was studied by means of confocal laser scanning microscopy (CLSM). The cells were seeded in a 6-well plate and

View Article Online
DOI: 10.1039/C5RA09931E

allowed to attach for 24h. The cells were then exposed with rhodamine-b loaded NP and M-NP and incubated for 1h. After washing with PBS, cells were stained with Lysotracker Green for lysosomes. The cells were fixed with 4% paraformaldehyde and washed. The cells were again stained with DAPI as a nuclear staining dye. The cellular internalization process was investigated using confocal microscope (Nikon, Japan).

Pharmacokinetic and biodistribution study

Male Balb/c mice, 4–5 weeks old, weighing 10–20 g was selected to perform the pharmacokinetic analysis. The animal study protocol was approved (Ref no. 2015ANZQ268) by Institutional Animals Ethical Committee (IAEC), Shandong Cancer Hospital and Institute, China. The entire study was carried out in accordance with the standard institutional guiding principles of IAEC. As per the reported protocol, A549 tumors were generated on the right flank of mice. The mice were divided into 3 groups with 6 mice in each group. The free Gnb, NP-Gnb, and M-NP-Gnb were administered at a fixed dose of 5 mg/kg via tail vein. For biodistribution study, animals were sacrificed at specific time intervals and tumor was extracted and stored at -80°C until further analysis. For pharmacokinetic assay, blood samples were collected and centrifuged at 5000rpm for 10 min and plasma was separated. To 100 µl of plasma, 100 µl of acetonitrile was added and protein was precipitated. The drug was extracted from the organic mixture using centrifugation. The supernatant was collected, filtered through 0.45 µm filter and injected into the HPLC column. The amount of drug present in the blood as well as in the individual organ was determined using HPLC method.

View Article Online
DOI: 10.1039/C5RA09931E

Statistical analysis

Statistical analysis of the data was performed using SPSS 16.0 (SPSS Corp., USA) with one-way ANOVA followed by Tukey's post hoc test. $P<0.05$ was considered statistically significant. The data are presented as mean±SD.

Conclusion

In this study, we have successfully prepared a mannose-conjugated pH-sensitive nanosystem for the effective delivery of Gefitinib to lung cancer cells. We have successfully demonstrated the prospective of mannose-tagged nanomicelles as an efficient vector to ferry anticancer drug. The micelles exhibited a nanosized particle with excellent dispersity index. The nanomicelles exhibited a pH-responsive nature with enhanced drug release in the acidic pH conditions. The fluorescence and flow cytometer analysis showed a superior cellular uptake for mannose-tagged nanomicelles. The CLSM study revealed a receptor-mediated cellular internalization process. The M-NP-Gnb showed a superior anticancer effect in A549 cancer cells and remarkably inhibited the cancer cell proliferation. Furthermore, M-NP-Gnb significantly increased the proportion of cells in the apoptosis and necrosis region. Importantly, half-life of Gnb encapsulated in nanomicelles increased by about 5-fold comparing to that of free Gnb. The augmented half-life clearly indicates the maximum residence time of drug in the systemic circulation. Consistently, M-NP-Gnb showed a 7-fold higher accumulation of drug in tumor tissues compared to that of free Gnb. Overall; PLGA/His-based nanomicelles could be a promising delivery system to increase the therapeutic efficiency of Gnb in lung cancers.

View Article Online
DOI: 10.1039/C5RA09931E

Acknowledgement

This work supported by Traditional Chinese medicine science and technology development plan of Shandong Province（No. 2013-208).

References

1. R. Siegel, J. Ma, Z. Zou, A. Jemal, *CA Cancer J. Clin*. 2014, **64**, 9–29.
2. C.G. Azzoli, S. Baker, S. Temin S, et al, *J. Clin. Oncol.* 2009, **27**, 6251–6266.
3. A. Jemal, F. Bray, M.M. Center, J. Ferlay, E. Ward, D. Forman, *CA Cancer J. Clin*. 2011, **61**, 69.
4. D.M. Parkin, F. Bray, J. Ferlay, P. Pisani, *CA Cancer J. Clin*. 2005, **55**, 74–108.
5. H. Wao, R. Mhaskar, A. Kumar, B. Miladinovic, B. Djulbegovic, *Syst. Rev*. 2013, **2**, 10.
6. S.M. Thomas, J.R. Grandis, *Cancer Treat. Rev*. 2004, **30**, 255–268.
7. T. Kosaka, Y. Yatabe, H. Endoh, K. Yoshida, T. Hida, M. Tsuboi, H. Tada, H. Kuwano, T. Mitsudomi, *Clin. Cancer Res*. 2006, **12**, 5764–5769
8. J. Hyung Park, S. Kwon, M. Lee, H. Chung, J.H. Kim, Y.S. Kim, R.W. Park, I.S. Kim, S. Bong Seo, I.C. Kwon, S. Young Jeong, *Biomaterials* 2006, **27**,119–126.
9. A. Morabito, R. Costanzo, A.M. Rachiglio, R. Pasquale, C. Sandomenico, R. Franco, A. Montanino, E. De Lutio, G. Rocco, N. Normanno, *J. Thorac. Oncol.* 2013, **8**, e59–e60.
10. J. Ozao-Choy, G. Ma, J. Kao, G.X. Wang, M. Meseck, M. Sung, M. Schwartz, C.M. Divino, P.Y. Pan, S.H. Chen, *Cancer Res.* 2009, **69**, 2514–2522.
11. H. Chen, Y. Zhao, H. Wang, G. Nie, K. Nan, Curr. Drug Metab. 2012, **13**, 1087–1096.
12. F. Danhier, O. Feron, V. Préat, *J. Control. Rel.* 2010, **148**, 135–146.

View Article Online
DOI: 10.1039/C5RA09931E

13. V.P. Torchilin, *Adv. Drug Deliv. Rev*. 2012, **64**, 302–315.

14. D. Kim, E.S. Lee, K.T. Oh, Z.G. Gao, Y.H. Bae, *Small* 2008a, **4**, 2043–2050.

15. D. Kim, E.S. Lee, K. Park, I.C. Kwon, Y.H. Bae, *Pharm. Res*. 2008b, **25**, 2074–2082.

16. L. Zhang, F.X. Gu, J.M. Chan, A.Z. Wang, R.S. Langer, O.C. Farokhzad, *Clin. Pharmacol. Ther*. 2008, **83**, 761–769.

17. D. Peer, J.M. Karp, S. Hong, O.C. Farokhzad, R. Margalit, R. Langer, *Nat. Nanotechnol* 2007, **2**, 751–60.

18. M.E. Davis, Z. Chen, D.M. Shin, *Nat. Rev. Drug Discovery* 2008, **7**, 771–82.

19. S. Jain, S.P. Vyas, *J. Liposome Res*. 2006, **16**, 331–34.

20. A. Nag, R.C. Ghosh, *J. Drug Target*. 1999, **6**, 427–438

21. K. Osada, K. Kataoka, *Adv. Polym. Sci*. 2006, **202**, 113–53.

22. P. Agrawal, U. Gupta, N.K. Jain, *Biomaterials* 2007, **28**, 3349–3359.

23. M.D. Chavanpatil, A. Khdair, J. Panyam, *Pharm. Res*. 2007, **24**, 803–810.

24. A. Miglietta, R. Cavalli, C. Bocca, L. Gabriel, M.R. Gasco, *Int. J. Pharm*. 2000, **210**, 61–67.

25. H.B. Ruttala, Y.T. Ko, *Pharm. Res*. 2015, **32**, 1002-16.

26. M. Nahar, N.K. Jain, *Pharm. Res*. 2015, **26**, 2588-98.

27. E.S. Lee, K. Na, Y.H. Bae, *J. Control. Rel*. 2003, **91**, 103-113.

View Article Online
DOI: 10.1039/C5RA09931E

Figure captions

Figure 1: Synthesis of PLGA-PEG-NH2, Histidine-PEG, PLGA-PEG-Mannose.

Figure 2: Characterization of drug-loaded nanoparticles. (a) Particle size distribution of M-NP-Gnb, (b) transmission electron microscope (TEM) of M-NP-Gnb.

Figure 3: Release profile of NP-Gnb and M-NP-Gnb in phosphate buffered saline (pH 7.4) and acetate buffered saline (pH 5.5). The release study was performed at 37°C (containing 0.1% Tween 80).

Figure 4: Cellular uptake study on A549 cells. (a) Fluorescence analysis of NP-Gnb and M-NP-Gnb in cancer cells. The cellular uptake analysis was performed at various time points (b) flow cytometer analysis of NP-Gnb and M-NP-Gnb.

Figure 5: Cellular internalization of NP-Gnb and M-NP-Gnb in A549 cancer cells. The cells were stained with Lysotracker Green (green color) and DAPI (blue color).

Figure 6: (a) Cytotoxic effect of free Gnb, NP-Gnb and M-NP-Gnb in A549 cancer cells. The cells were incubated for 24h (a) and 48h (b) at 37°C. The cytotoxic effect of individual formulations was evaluated by means of MTT assay.

Figure 7: Annexin V/PI-based apoptosis assay via flow cytometer (FACS). Annexin V was used for apoptosis analysis and PI was used for necrosis analysis.

Figure 8: (a) Plasma concentration-time profile of free Gnb, NP-Gnb and M-NP-Gnb. The study was carried up to 24h. The Gnb was administered at a fixed dose of 5 mg/kg via tail vein. (b) Biodistribution of free Gnb, NP-Gnb and M-NP-Gnb in tumors at various time intervals up to 24h.

View Article Online
DOI: 10.1039/C5RA09931E

Table 1: pH-sensitive nature of M-NP-Gnb by DLS analysis

pH	Size (nm)	PDI	Zeta potential (mV)
8.5	146.8±2.16	0.118±0.018	-24.5±1.65
7.4	165.7±1.68	0.157±0.025	-18.2±1.12
6.5	210.2±2.61	0.265±0.034	-8.32±1.89
5.5	325.5±4.65	0.398±0.042	-3.26±1.46

View Article Online
DOI: 10.1039/C5RA09931E

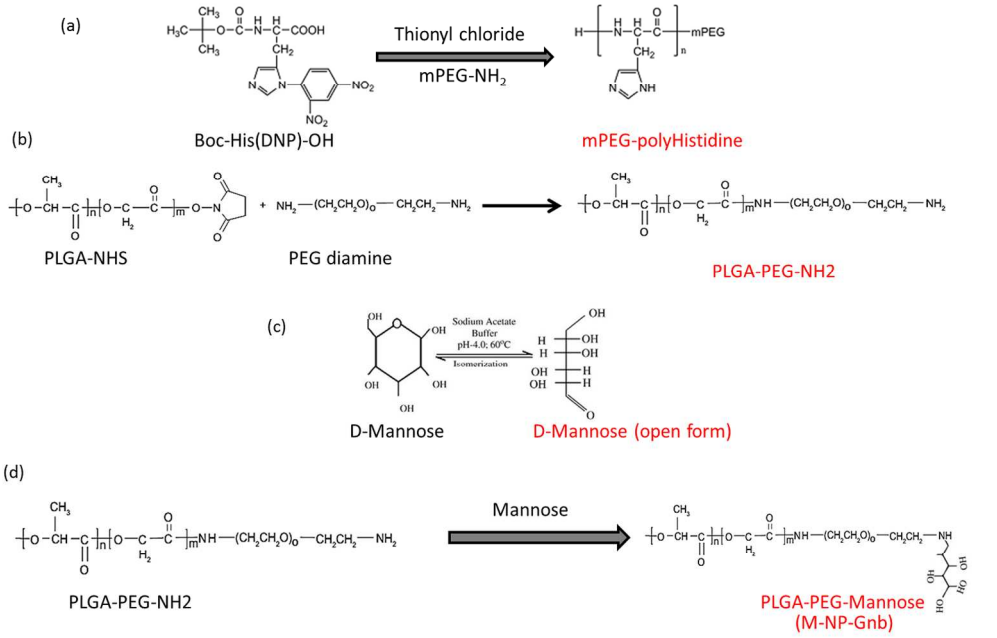

Figure 1
260x170mm (300 x 300 DPI)

View Article Online
DOI: 10.1039/C5RA09931E

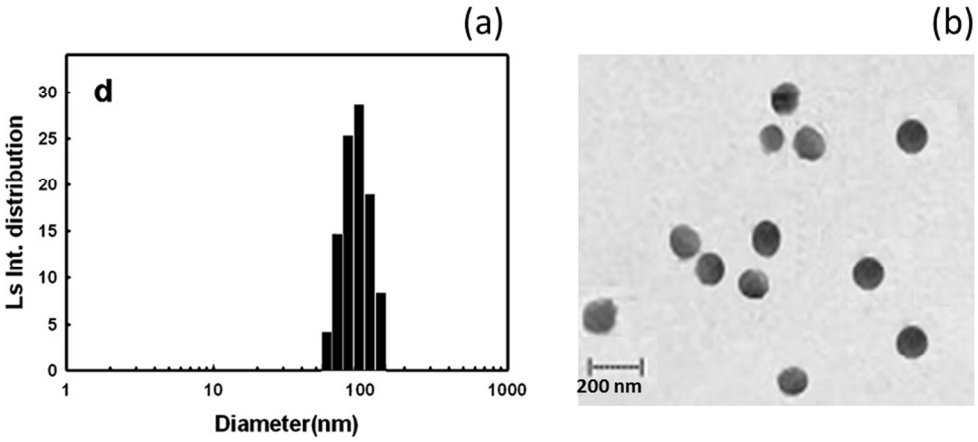

Figure 2
167x73mm (300 x 300 DPI)

View Article Online
DOI: 10.1039/C5RA09931E

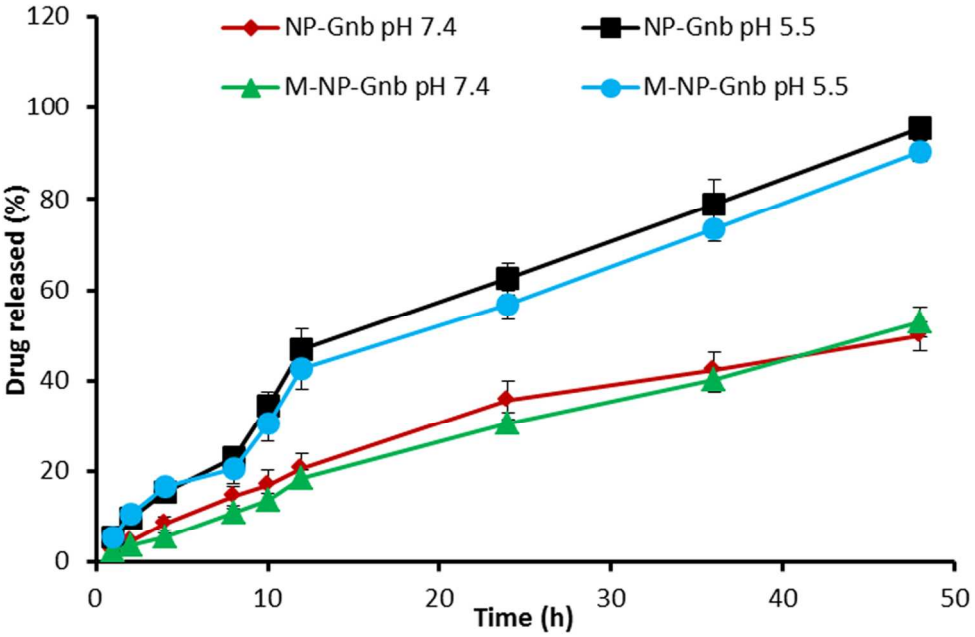

Figure 3
123x79mm (300 x 300 DPI)

View Article Online
DOI: 10.1039/C5RA09931E

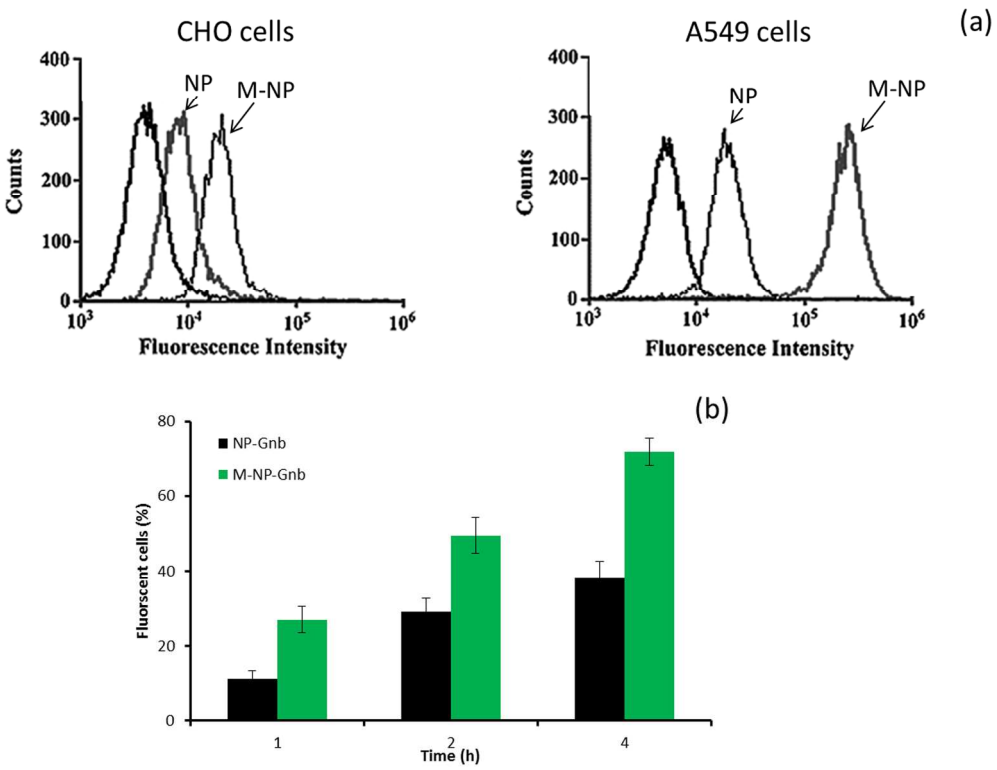

Figure 4
208x159mm (300 x 300 DPI)

View Article Online
DOI: 10.1039/C5RA09931E

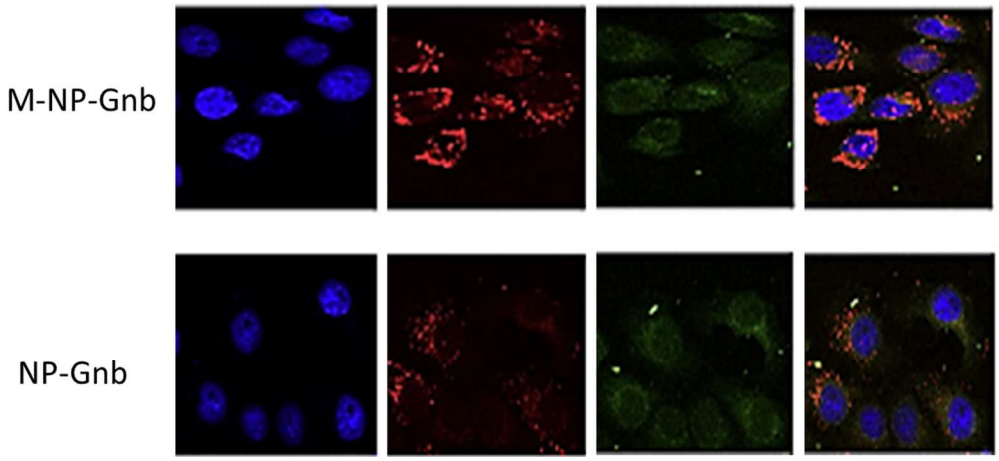

Figure 5
185x88mm (300 x 300 DPI)

View Article Online
DOI: 10.1039/C5RA09931E

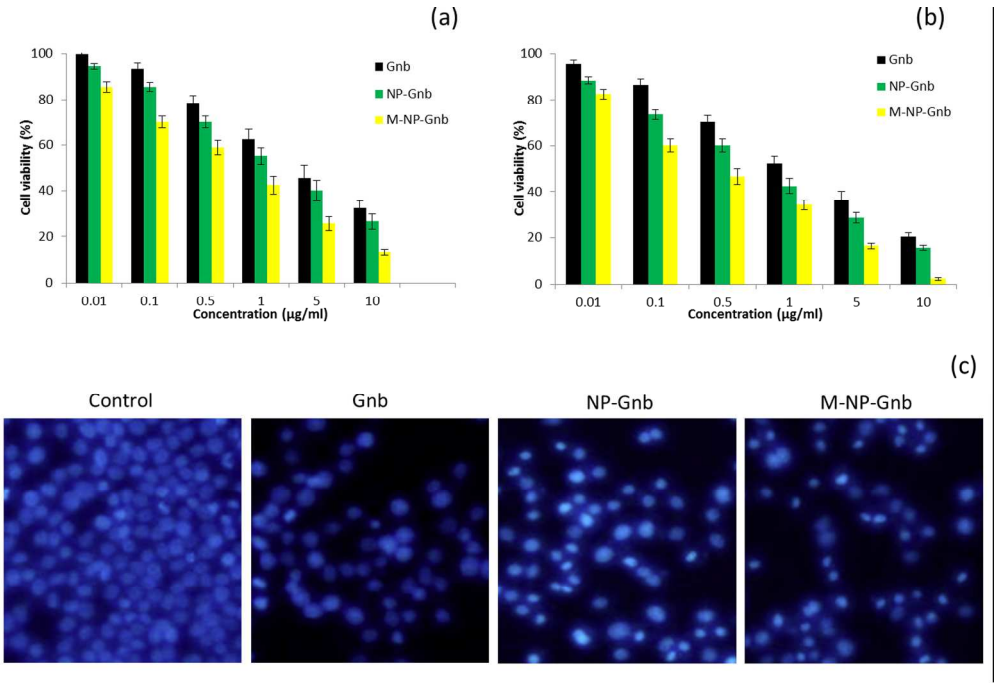

Figure 6
244x164mm (300 x 300 DPI)

View Article Online
DOI: 10.1039/C5RA09931E

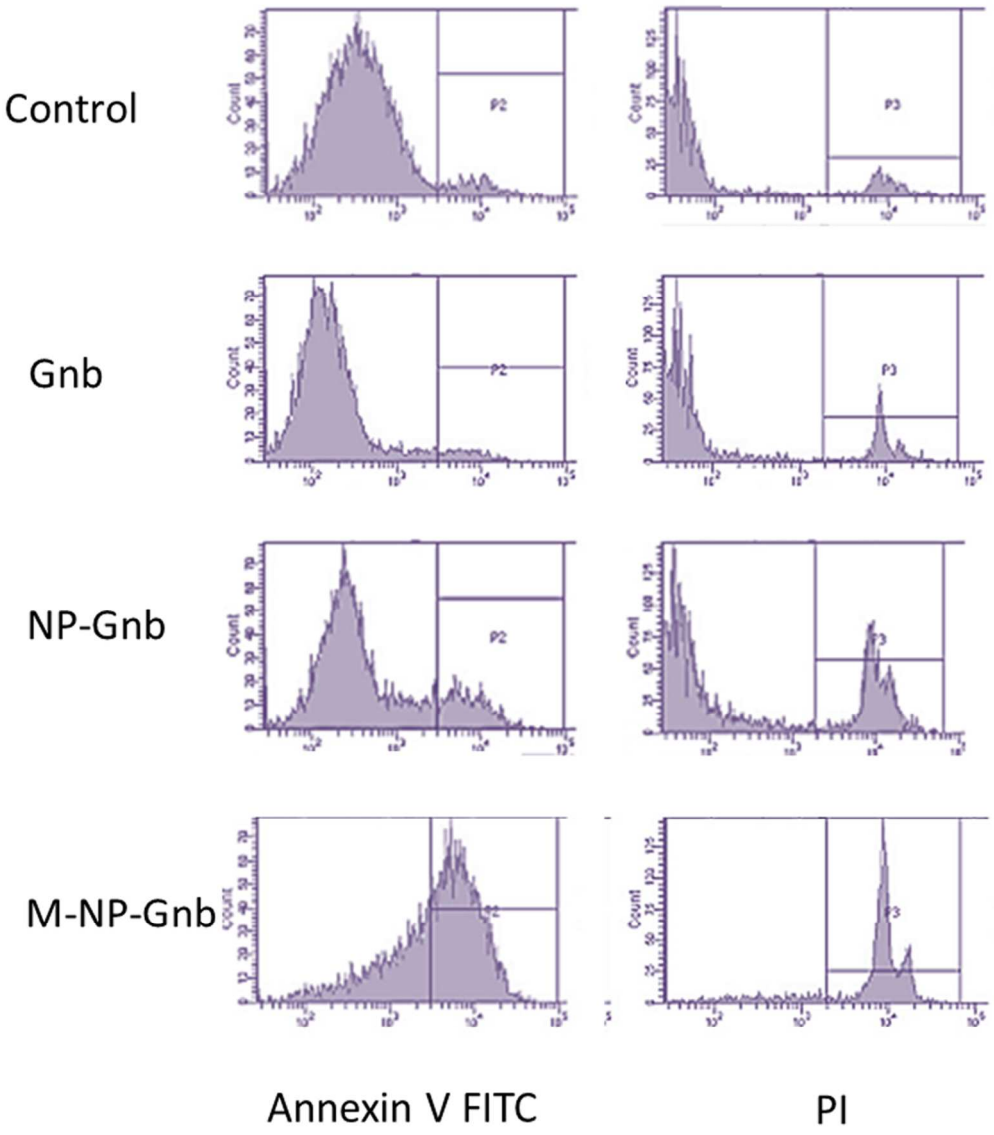

Figure 7
117x134mm (300 x 300 DPI)

View Article Online
DOI: 10.1039/C5RA09931E

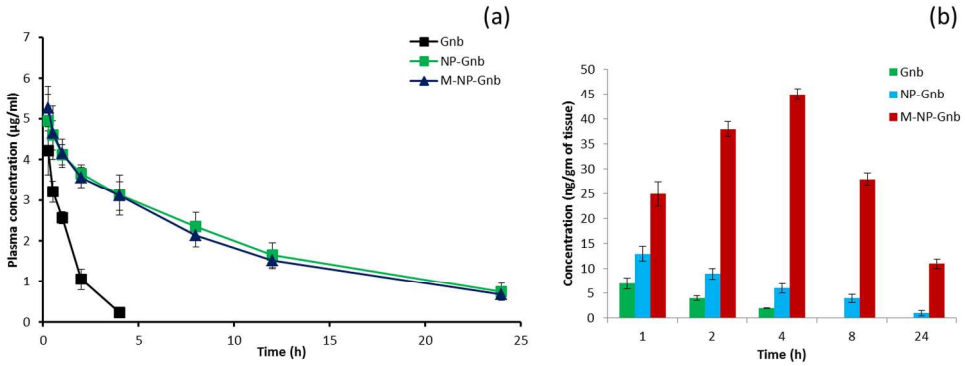

Figure 8
251x93mm (300 x 300 DPI)

View Article Online
DOI: 10.1039/C5RA09931E

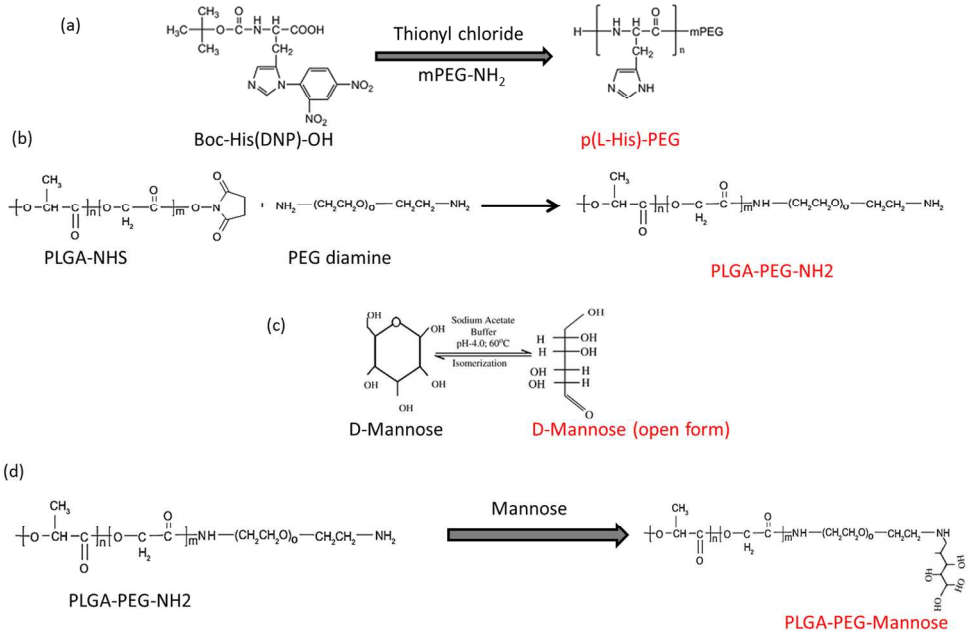

Graphical Abstract
260x167mm (300 x 300 DPI)